Six- to Five-Coordinate Heme−Nitrosyl Conversion in Cytochrome *c′* and Its Relevance to Guanylate Cyclase†

Colin R. Andrew,*,‡,§ Simon J. George,|| David M. Lawson,|| and Robert R. Eady||

Department of Chemistry, Eastern Oregon University, One University Boulevard, La Grande, Oregon 97850-2899, Department of Biochemistry and Molecular Biology, Oregon Graduate Institute of Science and Technology, 20000 NW Walker Road, Beaverton, Oregon 97006-8921, and Department of Biological Chemistry, John Innes Centre, Norwich NR4 7UH, U.K.

Received July 9, 2001

ABSTRACT: The 5-coordinate ferrous heme of *Alcaligenes xylosoxidans* cytochrome *c′* reacts with NO to form a 6-coordinate nitrosyl intermediate (λ_{Soret} at 415 nm) which subsequently converts to a 5-coordinate nitrosyl end product (λ_{Soret} at 395 nm) in a rate-determining step. Stopped-flow measurements at pH 8.9, 25 °C, yield a rate constant for the formation of the 6-coordinate nitrosyl adduct, $k_{on} = (4.4 \pm 0.5) \times 10^4$ M^{-1} s^{-1}, which is 3−4 orders of magnitude lower than the values for other pentacoordinate ferrous hemes and is consistent with NO binding within the sterically crowded distal heme pocket. Resonance Raman measurements of the freeze-trapped 6-coordinate nitrosyl intermediate reveal an unusually high Fe−NO stretching frequency of 579 cm^{-1}, suggesting a distorted Fe−N−O coordination geometry. The rate of 6- to 5-coordinate heme nitrosyl conversion is also dependent upon NO concentration, with a rate constant, $k_{6-5} = (8.1 \pm 0.7) \times 10^3$ M^{-1} s^{-1}, implying that an additional molecule of NO is required to form the 5c-NO adduct. Since crystallographic studies have shown that the 5-coordinate nitrosyl complex of cytochrome *c′* binds NO to the proximal (rather than distal) face of the heme, the NO dependence of the 6- to 5-coordinate NO conversion supports a mechanism in which the weakened His ligand, as well as the distally bound NO, is displaced by a second NO molecule which attacks and is retained in the proximal coordination position. The fact that a dependent 6- to 5-coordinate nitrosyl conversion has been previously reported for soluble guanylate cyclase suggests that the mechanism of Fe−His bond cleavage may be similar to that of cytochrome *c′* and strengthens the recent proposal that both proteins exhibit *proximal* NO binding in their 5-coordinate nitrosyl adducts.

Nitric oxide (NO)[1] is implicated as a signaling molecule in a wide range of organisms including animals, plants, and micoorganisms (*1*−*7*). The best characterized system is that of animals, in which cell−cell signaling occurs through the interaction of micromolar NO levels with the heme-containing enzyme, soluble guanylate cyclase (sGC) (*8*). Binding of NO to the heme center of sGC triggers the conversion of GTP to the second-messenger cGMP, which in turn regulates a host of physiological processes such as smooth muscle contraction, blood clotting, and neurotransmission (*2*, *8*). Formation of a 5c-NO heme complex in sGC and the associated Fe−His bond cleavage are believed to be the trigger which activates the production of cGMP (*8*, *9*). Deducing the mechanism of 5c-NO adduct formation in sGC is, therefore, of particular biomedical interest.

Cytochrome *c′* (cyt *c′*) is a hemoprotein found in the periplasm of certain proteobacteria which contains a pentacoordinate heme center located toward the C-terminus of a four α-helix bundle (*10*, *11*). Although the exact physiological role of cyt *c′* is unclear, several studies have suggested that NO binding to the heme may help bacteria suppress potentially toxic levels of free NO in their environment (*12*−*16*). In particular, Moir and co-workers have shown that a cyt *c′*-deficient mutant of the photosynthetic bacterium *Rhodobacter capsulatus* exhibited increased sensitivity to nitrosative stress (*16*). Intriguingly, the same group recently reported in vivo studies suggesting that *R. capsulatus* cyt *c′* might in fact function as an NO reductase (*17*).

Additional interest in the coordination chemistry of cyt *c′* stems from similarities with sGC, including the ability to form a 5c-NO heme adduct (*18*). Moreover, recent crystallographic characterization of cyt *c′* from *Alcalignes xylosoxidans* (AXCP) has yielded the exciting discovery that exogenous ligands are able to bind to the Fe from either side of the heme face. Whereas the 6c-CO complex of AXCP contains CO bound to Fe at the distal position, the 5c-NO adduct exhibits a novel proximal coordination geometry with NO residing at the site originally occupied by the His ligand (*19*). In the case of sGC, the currently accepted model for

†This work was supported by NIH Grant GM 34468 to Professor Thomas M. Loehr. D.M.L., S.J.G., and R.R.E. are funded by the BBSRC as part of the competitive strategic grant to the John Innes Centre.

* To whom correspondence should be addressed. Fax: (541) 962-3873. E-mail: candrew@eou.edu.

‡ Present address: Eastern Oregon Univeristy.

§ Oregon Graduate Institute of Science and Technology.

|| John Innes Centre.

[1] Abbreviations: NO, nitric oxide; CO, carbon monoxide; 5c and 6c, 5-coordinate and 6-coordinate, respectively; cyt *c′*, cytochrome *c′*; AXCP, *Alcaligenes xylosoxidans* cyt *c′*; cyt *c*, mitochondrial cytochrome *c*; sGC, soluble guanylate cyclase; Mb, myoglobin; Hb, hemoglobin; CCP, cytochrome *c* peroxidase; CooA, CO oxidation activator; PGHS-1, prostaglandin endoperoxide H synthase-1; NOS, nitric oxide synthase; P450, cytochrome P450; CPO, chloroperoxidase.

10.1021/bi011419k CCC: $22.00
Published on Web 01/25/2002

NO-induced activation assumes NO binding at the distal position in 5c-NO adduct (*9*). Clearly, the novel proximal heme−NO geometry in AXCP has potential implications for the mechanism of NO sensing and signal transduction in sGC if the latter were also to exhibit a proximal NO coordination.

A further shared property of AXCP and sGC is that they both form a 6c-NO intermediate (with the proximal His ligand intact) prior to the 5c-NO end product. In the case of sGC, the 6c-NO species has been observed using EPR and UV−vis spectroscopy (*20*, *21*). Interestingly, the rate of 6c- to 5c-NO conversion in sGC has been shown to be first order with respect to NO concentration, suggesting that cleavage of the Fe−His bond in the 6c-NO adduct requires the interaction of a second NO molecule somewhere on the protein. Recently, we identified a 6c-NO intermediate in AXCP using time-resolved FTIR spectroscopy (*22*). We also observed that the rate at which the 6c-NO species converted to the 5c-NO end product increased at higher NO concentrations. In the present study we report UV−vis stopped-flow kinetics of NO binding to AXCP under pseudo-first-order conditions, as well as the characterization of the 6c-NO intermediate using resonance Raman (RR) spectroscopy. Our results suggest a novel mechanism for 5c-NO heme formation and provide further evidence that AXCP is a useful paradigm for NO binding to sGC.

MATERIALS AND METHODS

AXCP was purified using procedures similar to those described previously (*23*, *24*). Heme concentrations were determined from electronic absorption measurements using previously reported absorptivities (*25*). Reduction to the ferrous state was achieved by the addition of an ∼10-fold excess of a sodium dithionite or electrochemically reduced methyl viologen solution. Excess reductant was removed using a P-6 desalting gel (Bio-Rad). Aqueous solutions of NO were prepared inside a gastight syringe by equilibrating approximately equal proportions of anaerobic buffer with either ^{14}NO (Aldrich) or ^{15}NO (98% ^{15}N; Cambridge Isotope Laboratory) gas which had been treated with 0.1 M KOH solution to remove higher oxides of nitrogen. The concentration of a saturated NO solution was assumed to be 2 mM at 1 atm of pressure.

UV−vis absorption spectra were recorded using either a Perkin-Elmer lambda 9 or Cary 50 rapid-scan spectrophotometer. Stopped-flow kinetic measurements were performed using a Hi-Tech SF-61 DX2 double-mixing stopped-flow spectrometer interfaced with a CU-61 control unit (Hi-Tech Scientific) operating in single-wavelength photomultiplier mode. The optical flow cell had a path length of 10 mm, and the dead time before detection was ∼2 ms. An anaerobic glovebox (Faircrest Ltd.) (<10 ppm of O_2) entirely housed the drive syringes and optical cell, and both the glovebox atmosphere and drive system were thermostated to give a sample temperature of 25 °C. Reactions of ferrous AXCP with NO were carried out under pseudo-first-order conditions in buffered solutions at pH 8.9. The KinetAsyst 2.2 software package (Hi-Tech Scientific) was used to analyze NO binding kinetics.

Resonance Raman (RR) spectra were recorded on a custom McPherson 2061/207 spectrograph (set to 0.67 m) equipped with a Princeton Instruments liquid N_2-cooled (LN-1100PB) CCD detector. Excitation at 413.1 nm was provided by a Kr ion laser (Innova 302). A Kaiser supernotch filter was used to attenuate Rayleigh scattering from samples in an ∼135° backscattering geometry which were maintained at 90 K using a liquid N_2 dewar (*26*). Frequencies were calibrated relative to indene, aspirin, and CCl_4 as standards and are accurate to ±1 cm^{-1}. Freeze-trapped RR samples of hexacoordinate heme−NO adducts of AXCP were prepared by the introduction of an ∼2-fold excess of NO through a septum-sealed 5 mm diameter capillary containing argon-purged reduced protein. The identity of the resultant complex was checked by UV−vis spectroscopy within 30 s of mixing, and the sample was quickly frozen in liquid N_2.

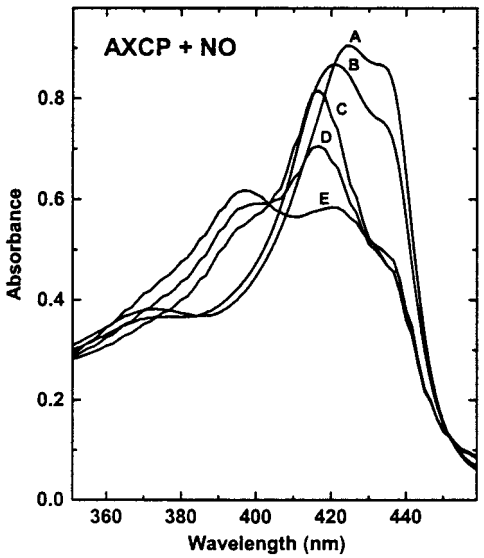

FIGURE 1: Effect of nonsaturating NO concentrations on the UV−vis absorption of ferrous AXCP:. (A) initial solution of 9 μM heme ferrous AXCP; (B) immediate effect of adding 5 μM NO to spectrum A; (C) immediate effect of adding 20 μM NO to spectrum B; (D and E), time-dependent changes in spectrum C recorded at 5 and 70 min, respectively, after the NO addition.

RESULTS

UV−Vis Absorption of the 6c-NO Intermediate. Since AXCP rapidly forms a 5c-NO heme adduct with NO in large excess, solutions of ferrous AXCP were titrated with small amounts of NO with the aim of trapping the 6c-NO intermediate. Although this approach increased the lifetime of the 6c-NO species, subsequent conversion to the 5c-NO adduct was always observed, even at substoichiometric NO concentrations. Figure 1 shows changes in Soret absorption which occur when nonsaturating amounts of NO are added to a 9 μM heme solution of ferrous AXCP. The initial addition of 5 μM NO AXCP (Figure 1A) causes a rapid shift in the Soret maximum from 424 to 421 nm, along with a slight decrease in intensity (Figure 1B). Subtraction of the absorption features of ferrous AXCP from Figure 1B yields a spectrum with a Soret maximum at 415 nm, together with α and β bands at 575 and 540 nm, respectively (Figure 2B), which we assign to that of the 6c-NO intermediate on the basis of the similarities with other 6c-NO ferrous hemes (Table 1). The presence of a weak shoulder near 395 nm in Figure 2B suggests that a small amount of 5c-NO heme is present along with the 6c-NO species. Further addition of NO to a total of 25 μM (∼3.0 equiv) shifts the heme Soret

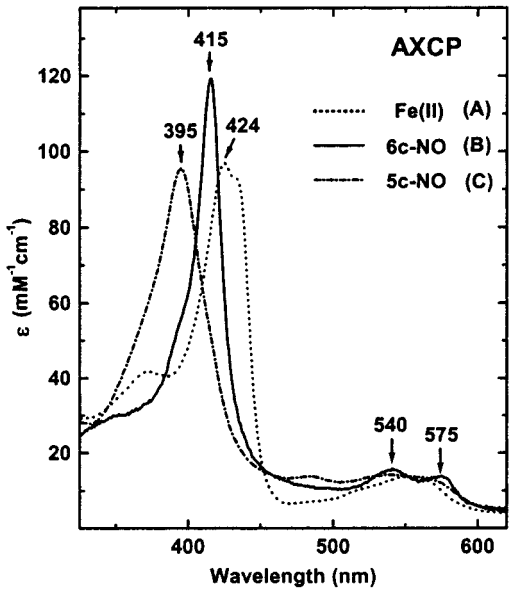

FIGURE 2: Electronic absorption spectra of solutions of (A) ferrous, (B) 6c-NO, and (C) 5c-NO AXCP in 50 mM Tris-HCl buffer, pH 8.9 at 25 °C. Molar absorptivities were calculated on the basis of previously reported values for ferrous heme (*25*).

Table 1: Electronic Absorption Parameters for Nitrosyl Adducts of Ferrous Hemoproteins

hemo-protein	λ_{max}, nm (ϵ, mM^{-1} cm^{-1})				ref
			6c-NO		
AXCP[a,b]	415 (120)		540	575	this work
sGC[a]	420		544	579	*20, 21*
Mb	420 (127)		548 (11.3)	579 (10.1)	*52*
CCP	421 (99)		542 (12)	572 (11)	*53*
cyt *c*	411 (127)		539 (10.2)	567 (9.8)	*54*
			5c-NO		
AXCP[b]	395 (95)	485 (13)	539 (14)	565 (13)	this work
AXCP	397 (78.9)	485 (9.8)	541 (10.4)	565 (10)	*55*
sGC	398 (75)	nr[c]	537 (12)	572 (12)	*18*
CooA	399	nr	544	572	*43*
PGHS-1	402	484	543	566	*49*

[a] Transient precursor to 5c-NO adduct. [b] Absorptivity calculated on the basis of previously reported values for ferrous heme (*25*). [c] nr, not reported.

to 415 nm (Figure 1C), consistent with substantial formation of the 6c-NO adduct. However, spectra recorded 5 and 70 min after mixing (Figure 1, spectra D and E, respectively) show a buildup of absorption near 395 nm at the expense of the peak near 415 nm, along with an isosbestic point near 405 nm, consistent with conversion of the 6c-NO species to the 5c-NO end product with its characteristic Soret maximum at 395 nm (Figure 2C). The final equilibrium mixture (Figure 1E) consists of 5c-NO and ferrous AXCP (with negligible amounts of the 6c-NO species), showing that the 6c-NO adduct is not stable with respect to these species.

Kinetics of NO Binding. Single-wavelength stopped-flow UV−vis absorption measurements were carried out to monitor the reaction of ferrous AXCP with excess NO under pseudo-first-order conditions. Figure 3 shows typical time courses for the reaction at 395, 408, and 424 nm. The overall increase in absorption at 395 nm, together with the decrease at 425 nm, is consistent with the generation of the 5c-NO heme at the expense of ferrous heme, while the growth and decay of absorption at 408 nm are consistent with the

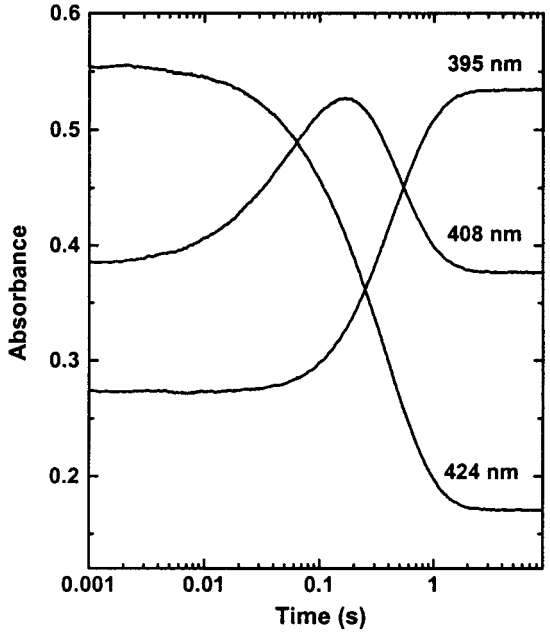

FIGURE 3: Stopped-flow time courses (solid line) at 395, 408, and 424 nm for the reaction of ferrous AXCP (5.9 μM in heme) with 300 μM NO in 50 mM bis-tris propane buffer and 100 mM NaCl, pH 8.9, 25 °C. Superimposed and largely obscured by each time course is a kinetic fit (dashed line) to two consecutive exponential processes with rate constants of k_{1obs} (∼11.7 s^{-1}) and k_{2obs} (∼2.6 s^{-1}) for the first and second steps, respectively. To facilitate the iterative fitting, k_{1obs} was initially set to twice the value of k_{2obs} determined from a single-exponential fit of the latter portion of the reaction.

formation and disappearance of the 6c-NO intermediate. Using an A → B → C kinetic model corresponding to ferrous (A), 6c-NO (B), and 5c-NO (C) forms of AXCP, each time course was fitted to two consecutive exponential processes to yield observed rate constants k_{1obs} and k_{2obs} for the first and second steps, respectively. Typical time courses are shown in Figure 3. The calculated rate constants exhibited no wavelength dependence over the range studied.

A linear plot of k_{1obs} vs NO concentration gives the second-order rate constant $k_{on} = (4.4 \pm 0.5) \times 10^4$ M^{-1} s^{-1} for the formation of the 6c-NO adduct (Figure 4). This value is 3−4 orders of magnitude lower than the NO association rate constants for other 5c hemoproteins such as Mb and sGC (Table 2), implying that NO binding to AXCP is associated with a relatively high degree of steric hindrance. Likewise, a previous study of CO binding to AXCP reported an unusually low CO association rate constant of 92 M^{-1} s^{-1} (*27*), which is 4 orders of magnitude lower than that of Mb. X-ray crystal structures of AXCP shed light on the reason for the slow rates of exogenous ligand binding (*19*). Not only is the distal face of the heme shielded from solvent, but the size of the distal cavity is unusually small due to the location of the Leu 16 residue directly above the Fe. In the case of CO binding to ferrous AXCP, the distal pocket undergoes a significant structural rearrangement involving the rotation of the Leu 16 side chain around the $C_\alpha-C_\beta$ bond, which in turn causes a flattening of the porphyrin ring (*19*). The kinetic barrier associated with this rearrangement most likely accounts for the particularly low rates of CO and NO binding. It is noted that a bulky hydrophobic group (from either Leu, Met, Phe, or Tyr) is present in the distal heme pockets of all known cytochromes *c*′ (*28*), suggesting that steric hindrance

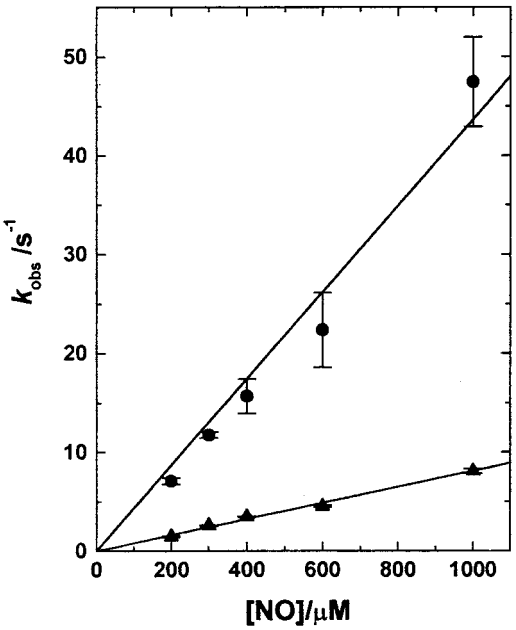

FIGURE 4: Dependence of k_{1obs} (circles) and k_{2obs} (triangles) on NO concentration. Values of k_{1obs} and k_{2obs} were obtained by fitting absorbance vs time traces to two consecutive exponential processes as described in Figure 3. Each data point is the mean of three separate fittings using time courses at 395, 408, and 424 nm, with error bars depicting the standard deviation. Linear plots of k_{obs} vs NO concentration, fitted through the origin, were used to calculate the second-order rate constants.

Table 2: Rate Constants for NO Binding to Ferrous Hemoproteins

hemoprotein	temp, °C	k_{on}, M^{-1} s^{-1}	k_{6-5}, M^{-1} s^{-1}	ref
AXCP	25	4.4×10^4	8.1×10^3	this work
sGC	4	$>1.4 \times 10^8$	2.4×10^5 [a]	*21*
sGC	15	$>1.7 \times 10^7$	*b*	*20*
β(1−385) sGC	4	7.1×10^8	*c*	*21*
Mb	20	1.7×10^7	*d*	*56*
cyt *c*	nr[e]	8.3	*d*	*57*

[a] First-order rate constant of 8.7×10^{-3} s^{-1} reported for substoichiometric amounts of NO. [b] First-order rate constant of ~38 s^{-1} reported for 60 μM NO. [c] 6c-NO intermediate not detected. [d] 5c-NO adduct formation observed at pH <4, presumably caused by protonation of the proximal His ligand (*58*, *59*). [e] Not reported.

to distal ligand binding may by functionally relevant.

As with the initial NO−heme binding step, the 6c- to 5c-NO conversion is also a second-order process (Figure 4), with a linear plot of k_{2obs} vs NO concentration yielding the rate constant $k_{6-5} = (8.1 \pm 0.7) \times 10^3$ M^{-1} s^{-1}. Considering that the X-ray crystal structure of the 5c-NO adduct shows NO bound to the proximal heme face, the NO dependence of the 6c- to 5c-NO kinetics points to a mechanism in which a second NO molecule attacks on the proximal side of the 6c-NO heme, to displace both the His ligand and the distally bound NO (Figure 5). An alternative mechanism, in which the rate-determining step of 5c-NO adduct formation is the spontaneous dissociation of the Fe−His bond, is ruled out by the second-order kinetics. Significantly, a recent kinetic study of NO binding to ferrous sGC also found the rate of 6c- to 5c-NO conversion to be first order with respect to NO concentration with $k_{6-5} = 2.4 \times 10^5$ M^{-1} s^{-1} at 4 °C (*21*) (Table 2). The present kinetic data for AXCP strengthen the analogies between cyt *c*′ and sGC and suggest that the latter could also bind NO to the proximal side of the heme.

Despite the NO dependence of k_{6-5}, our UV−vis studies of NO binding under nonsaturating conditions (vide infra) show that excess NO is not an absolute requirement for 5c-NO formation. Addition of substoichiometric amounts of NO to ferrous AXCP initially produces an equilibrium mixture of ferrous protein and 6c-NO adduct, which is then followed by slow conversion of the 6c-NO species to a 5c-NO adduct. The latter process may be due to a small equilibrium concentration of free NO in solution which reacts with the 6c-NO species via the mechanism shown in Figure 5. Alternatively, there may be an additional route for the 6c- to 5c-NO conversion in AXCP which is NO independent. In the case of sGC, a 5c-NO species is also formed at substoichiometric NO levels with a rate constant of 0.0087 s^{-1} (*21*).

RR Characterization of the 6c-NO Intermediate. RR measurements were carried out on the freeze-trapped 6c-NO complex of AXCP at 90 K to investigate the structure of the transient heme−NO moiety. Samples of the 6c-NO species were prepared by reacting ferrous AXCP with an ~2-fold excess of NO and then manually freezing in liquid N_2 within 30 s of mixing. UV−vis spectra of the samples recorded immediately prior to freezing (data not shown) revealed absorption maxima at 415, 540, and 575 nm, indicating that the protein was predominantly in the 6c-NO state and had not yet converted to the 5c-NO adduct. A shoulder near 425 nm also indicated the presence of unreacted ferrous heme.

RR spectra of frozen samples of AXCP were obtained using 413.1 nm excitation, yielding porphyrin marker bands in the 1350−1650 cm^{-1} region (Figure 6) whose frequency is characteristic of the Fe oxidation state, spin state, and coordination number (*29*). The RR spectrum of ferrous AXCP at 90 K (Figure 6A) resembles that previously observed at room temperature (Table 3) (*30*), with the increase in porphyrin marker band frequencies at low temperature attributable to a contraction of the heme core (*31*). RR spectra of the freeze-trapped nitrosyl complexes prepared with ^{14}NO (Figure 6B) and ^{15}NO (Figure 6C) clearly show contributions from unreacted ferrous protein. Subtraction of the ferrous AXCP RR contribution from spectra B and C in Figure 6 yields the vibrations of the 6c-^{14}NO (D) and 6c-^{15}NO (E) adducts, respectively. Porphyrin marker bands attributable to the 6c-NO adduct of AXCP are evident at 1375 cm^{-1} (ν_4), 1504 cm^{-1} (ν_3), 1597 cm^{-1} (ν_2), and 1638 cm^{-1} (ν_{10}), which are in line with values previously reported for 6c-NO complexes (Table 3). The particularly high ν_2 frequency is a characteristic feature of all cyt *c*′ RR spectra (*30*). No evidence of RR vibrations from 5c-NO (*30*) or ferric AXCP (*32*−*36*) is apparent in Figure 6, spectra D and E. Although the 5c-NO and 6c-NO adducts of AXCP at 90 K both give rise to the same ν_2 frequency at 1596 cm^{-1} (Table 3), the two coordination geometries can be clearly distinguished via their ν_3 and ν_{10} frequencies, which are 7 and 10 cm^{-1} lower, respectively, in the case of the 6c-NO species (Table 3).

Confirmation of the 6c-NO RR assignment in AXCP was obtained through the identification of characteristic vibrational frequencies within the Fe−NO moiety. The ν(N−O) vibration was identified by subtraction of the 6c-^{15}NO RR spectrum from the 6c-^{14}NO spectrum (inset of Figure 6) to reveal an isotope-sensitive band at 1624 cm^{-1}, which

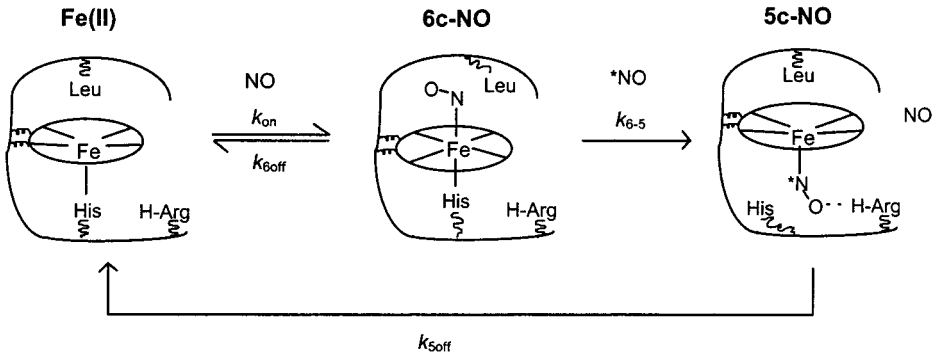

FIGURE 5: Proposed mechanism for the formation of ferrous−nitrosyl heme adducts in AXCP. First, NO binds to the sterically crowded distal coordination site of ferrous AXCP to form a transient 6c-NO complex with a labile proximal Fe−His bond. The 6c-NO complex is then converted to a proximally bound 5c-NO complex by reaction with a second NO molecule (*NO), which displaces the His ligand by direct attack and retention at the proximal position. The proximal 5c-NO geometry is stabilized by H-bonding with the nearby Arg 124 residue, as evident in the X-ray crystal structure.

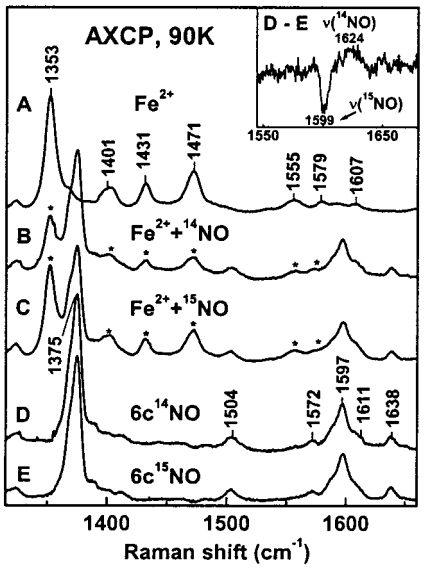

FIGURE 6: High-frequency RR spectra (413.1 nm excitation, 15 mW) obtained at 90 K for frozen solutions of ferrous AXCP (120 μM heme, pH 8.9) and freeze-trapped reaction products with NO: (A) ferrous AXCP; (B) ferrous AXCP reacted with ^{14}NO; (C) ferrous AXCP reacted with ^{15}NO. The RR spectra of 6c-NO AXCP shown in (D) and (E) were calculated by subtracting the spectral features of ferrous AXCP from (B) and (C), respectively. The inset shows the ^{14}NO − ^{15}NO difference spectrum (D − E). Protein samples were prepared by reacting ferrous AXCP (120 μM in heme) with ~250 μM NO and then freezing within 30 s.

downshifts to 1599 cm^{-1}. The 1624 cm^{-1} ν(N−O) frequency is typical for a 6c-NO heme (*37*, *38*), as compared to 5c-NO hemes which have ν(N−O) frequencies in the 1660−1703 cm^{-1} range (*39*). Moreover, the ν(N−O) assignment is in good agreement with a recent room temperature stopped-flow FTIR study of NO binding to ferrous AXCP in which a transient species with a ν(N−O) frequency of 1625 cm^{-1} is observed which downshifts to 1599 cm^{-1} with ^{15}NO (*22*). It is evident that the negative component of the ^{14}NO − ^{15}NO difference spectrum (Figure 6 inset) is narrower than the positive component, which may be due to coupling of the ν(^{15}N−O) vibration with the overlapping ν_2 mode at 1596 cm^{-1}, as previously described for nitrosyl-Mb (*37*). Coupling between these two modes might also account for the fact that the observed ^{14}NO−^{15}NO isotope shift in the 6c-NO RR spectrum (25 cm^{-1}) is less than the theoretical shift for the isolated N−O oscillator (29 cm^{-1}).

Table 3: Resonance Raman Frequencies (cm^{-1}) of 6- and 5-Coordinate Nitrosyl Adducts of Ferrous Hemoproteins

protein	temp, K	ν_3	ν_2	ν_{10}	ν(Fe−NO)	ν(N−O)	ref
			6c-NO				
AXCP	90	1504	1596	1638	579	1624	this work
Mb	293	1500	1583	1635	552[a]	1613	*37*
HbA	RT[b]	1500	1584	1636	551	1622	*60*
P450	273	1499	nr[c]	nr	554	1591	*61*
CPO	273	1502	nr	nr	542	nr	*62*
NOS	nr	nr	nr	nr	536,[d] 549[e]	nr	*63*
			5c-NO				
AXCP	RT[a]	1506	1592	1641	526	1661	*30*
AXCP	90	1511	1596	1648	nr	1661	this work
sGC[f]	293	1509	1583	1646	521	1681	*51*
sGC[f]	293−303	1509	1584	1646	525	1677	*50*
sGC[g]	RT	1508	1584	1645	520	no[h]	*64*
sGC[g]	nr	1508	1584	1644	no	1660	*42*
CooA	nr	1506	1582	1641	523	1672	*43*

[a] Value obtained from band-fitting simulation. [b] Room temperature. [c] Not reported. [d] Enzyme in the absence of substrate. [e] Enzyme in the presence of substrate. [f] Enzyme isolated with heme intact. [g] Enzyme reconstituted with heme. [h] Not observed.

To assign the ν(Fe−NO) vibration of the 6c-NO adduct of AXCP, RR spectra of the above samples were recorded in the low-frequency region (Figure 7). Unlike the high-frequency region (Figure 6), the low-frequency RR spectra of NO-containing samples (Figure 7, spectra A and B) appear to derive mainly from the 6c-NO heme with very little spectral contribution from ferrous protein (Figure 7C). Subtraction of the ^{15}NO-containing spectrum from that of the ^{14}NO sample identifies the ν(Fe−NO) at 579 cm^{-1} from its 15 cm^{-1} downshift. The magnitude of the isotope shift is close to the 16 cm^{-1} value expected for an isolated Fe−N oscillator. It is apparent that the ν(Fe−NO) frequency of AXCP is significantly higher than the values for other 6c-NO hemes which lie between 536 and 554 cm^{-1} (Table 3).

Previous studies of 6c-CO and 5c-NO complexes of ferrous hemes have shown that the frequencies of the ν(Fe−XO) and ν(X−O) vibrations are sensitive to back-bonding effects. Increased back-bonding from Fe(II) to the π* orbital of the exogenous ligand results in a stronger Fe−X bond (higher Fe−X stretch) and weaker X−O bond (lower X−O stretch), such that a plot of ν(Fe−XO) vs ν(X−O) will have a negative slope (*39*). In the case of 6c-NO heme complexes, FTIR studies have yielded a fair amount of data regarding ν(N−O) frequencies (see ref *38* and references cited therein), although there is scant RR data on the corresponding ν(Fe−

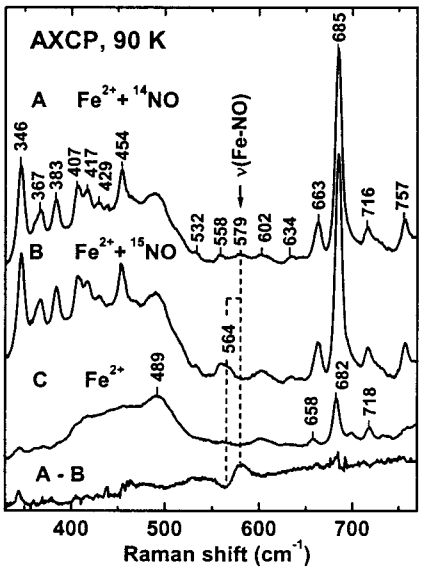

FIGURE 7: Low-frequency RR spectra (413.1 nm excitation, 15 mW) obtained at 90 K for frozen solutions of ferrous AXCP (120 μM heme, pH 8.9) and its freeze-trapped reaction products with 250 μM NO: (A) ferrous AXCP reacted with ^{14}NO; (B) ferrous AXCP reacted with ^{15}NO; (C) ferrous AXCP. The ^{14}NO − ^{15}NO difference spectrum (A − B) is depicted below. Spectra were obtained as described in Figure 6.

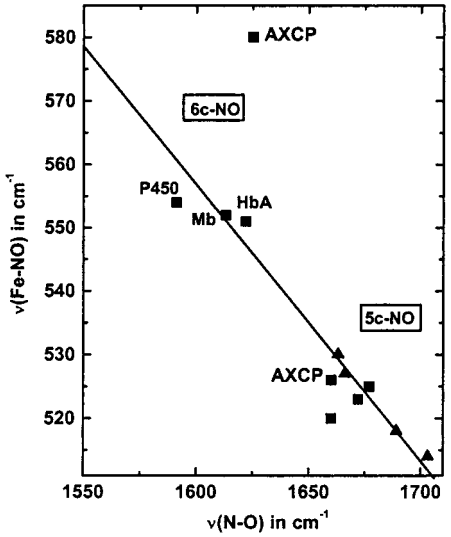

FIGURE 8: Plot of ν(Fe−NO) vs ν(N−O) frequencies for 5- and 6-coordinate NO adducts of ferrous hemes. The solid line indicates the back-bonding correlation established previously for NO adducts of porphyrin analogues (*39*). Data points are taken from Table 3 and ref *39*.

NO) vibrations due to the tendency of the Fe-bound NO to photodissociate in the laser beam (*39*). On the basis of the few ν(Fe−NO) values which exist in the literature for 6c-NO hemoproteins, Spiro and co-workers recently proposed that 6c-NO hemes exhibit the same back-bonding correlation as 5c-NO adducts, with the 6c-NO data shifted to lower ν(N−O) and higher ν(Fe−NO) values due to the additional back-bonding resulting from the presence of a proximal ligand (Figure 8). However, it can be seen that the data point for the 6c-NO adduct of AXCP does not lie on the same correlation line, suggesting that the electronic properties of the Fe−NO moiety differ from those of the other 6c-NO examples. What features of the AXCP heme could account for the unusually high ν(Fe−NO) frequency of the 6c-NO adduct?

RR studies of ferrous AXCP suggest that the His ligand has significant imidazolate character in the ferrous state (*30*, *36*), raising the possibility that the unusual ν(Fe−NO) frequency in the 6c-NO adduct of AXCP might be linked to the presence of a negatively charged proximal ligand. However, this appears unlikely since the RR studies of the 6c-CO adduct indicate that the His ligand is in fact neutral when the heme is hexacoordinate (*30*). Furthermore, Spiro and co-workers have argued that the back-bonding correlation for 6c-NO hemes is not significantly affected by the charge of the proximal ligand since, as shown in Figure 8, the data point for P450 (thiolate ligation) lies close to those of Mb and Hb (imidazole ligation) (*39*).

Given the steric crowding which exists within the distal heme pockets of AXCP, the most likely origin of the unusual ν(Fe−NO) frequency of the 6c-NO adduct would appear to lie with distortion of the Fe−N−O angle and/or tilting of the Fe−NO bond. The X-ray crystal structure of the distally bound 6c-CO complex shows that coordination of the exogenous ligand requires significant displacement of the Leu 16 side chain, which in turn could result in conformational strain within the Fe−CO moiety. Although the Fe−C−O angle of 167° does not deviate significantly from that of other heme−CO complexes, it has been proposed that the geometries of Fe(II)−nitrosyl complexes are much more easily perturbed by the surrounding heme pocket (*40*). Spiro and co-workers argued that ν(Fe−NO) frequencies increase as the Fe−N−O angle decreases (*39*), consistent with the 6c-NO adduct in AXCP having an Fe−N−O angle well below the typical value of ∼140° exhibited by unhindered Fe(II)−NO hemes.

DISCUSSION

Implications for NO Binding to sGC. The most significant finding of the present study is the second-order nature of the 6c- to 5c-NO conversion in AXCP. To our knowledge, the only other example in which a transient 6c-NO heme has been identified prior to the formation of a 5c-NO adduct is that of sGC (*20*, *21*, *41*). Although previous studies reported variations in kinetic behavior, Marletta and co-workers recently observed that the rate of 6c- to 5c-NO conversion was first order with respect to NO concentration with $k_{6-5} = 2.4 \times 10^5$ M^{-1} s^{-1} at 4 °C (Table 2) (*21*). It was proposed that the NO dependence of the 6c- to 5c-NO transition in sGC has functional relevance, since it would determine how much enzyme is activated at a given time, as well as how fast the enzyme is activated (*21*).

Accounting for the second-order kinetics of the 6c- to 5c-NO conversion in sGC has proved difficult to date. We propose, by analogy with AXCP, that the 6c-NO intermediate of sGC reacts with an additional NO molecule which attacks and is retained on the proximal side of the heme. While the attack of NO on the proximal heme face of sGC has been previously suggested (*21*), it has always been assumed that the final resting place for NO in the 5c-NO adduct was on the distal side of the heme. However, the similarities between the NO binding properties of sGC and AXCP strongly suggest that sGC could retain NO on the proximal side of its heme in the 5c-NO adduct. This alternative view of

proximal NO binding to sGC has tremendous implications for the nature of the conformational changes which lead to enzyme activation.

Additional evidence for a proximal NO−heme geometry in both AXCP and sGC exists from RR studies. In particular, RR spectra of the crystallographically characterized 6c-CO and 5c-NO adducts of AXCP indicate that the CO and NO ligands experience different electrostatic environments, consistent with their binding in the distal and proximal heme pockets, respectively (*30*). Intriguingly, RR studies of sGC are also consistent with different electrostatic environments for the 6c-CO and 5c-NO complexes, raising the possibility that CO and NO could also occupy opposite sides of the heme (*42*). It has been proposed that the latter scenario could account for the selective responses of sGC toward NO and CO (*30*).

Factors Influencing 5c-NO vs 6c-NO Coordination. It is clear that the coordination number of a hemoprotein−nitrosyl complex can have functional implications (*21*, *43*). What structural factors determine whether ferrous hemes form 5c- or 6c-NO adducts? In the case of simple heme complexes, the 5c-NO geometry is predominant due to the action of the repulsive trans effect (*44*, *45*). Protein systems are the exception due to the surrounding polypeptide which acts to resist the dissociation of the amino acid axial ligand, leading to most ferrous hemoprotein−NO adducts being hexacoordinate (*46*). However, the situation is not clear-cut, since some hemoproteins readily form 5c-NO adducts or else equilibrium mixtures of both 5c-NO and 6c-NO adducts (*47*, *48*).

The identification of a 6c-NO intermediate in both AXCP and sGC has implications for the previously established correlations between Fe−His bond strength and 5c-NO heme formation. A widely held view is that hemoproteins which form 5c-NO adducts are characterized by a weak or strained heme-proximal linkage in the ferrous state as evidenced by a low frequency for the Fe−His stretching vibration, ν(Fe−His) (*49*). For example, the ability of sGC to form a 5c-NO heme has been linked to its low ν(Fe−His) frequency of ~204 cm^{-1} (*50*, *51*). At first glance, the heme center in AXCP appears to behave anomalously since it reacts with NO to form a 5c-NO adduct, despite its relatively high ν-(Fe−His) frequency of 231 cm^{-1} (*30*). However, in analyzing these correlations it must be remembered that RR spectroscopy can only detect ν(Fe−His) frequencies of pentacoordinate ferrous hemes. In the case of AXCP and sGC, the existence of the 6c-NO intermediate prior to Fe−His bond cleavage implies that it is the Fe−His bond strength of the 6c-NO heme (rather than of the 5c-ferrous state) which influences 5c-NO heme formation. Thus, RR properties of the ferrous state may not always predict the Fe−His bond strength in the 6c-NO heme precursor, which in turn may account for the anomalous ν(Fe−His) frequency in AXCP.

In addition to the Fe−His bond strength, another means of controlling the heme−nitrosyl coordination number is suggested by the ability of AXCP to bind exogenous ligands to either face of its heme center. In this case, the driving force for the 6c- to 5c-NO transition may be associated with increased stabilization of proximally bound NO relative to distally bound NO. Crystallographic and spectroscopic data reveal that the proximally bound NO is strongly H-bonded to the Arg 124 residue, whereas no H-bond donors are present in the distal heme pocket (*19*, *22*, *30*). Interestingly, RR studies of the 6c-CO and 5c-NO complexes of sGC point to differences in the electrostatic environments of the two exogenous ligands, which could be due to their binding to opposite sides of the heme (*42*). Unlike the 5c-NO adduct of sGC, the heme pocket of the 6c-CO complex appears to be negatively polarized, which would tend to destabilize exogenous ligand binding. Thus, it is conceivable that the driving force for the 6c- to 5c-NO transition in sGC arises from NO binding on the opposite side of the heme to access a more favorable electrostatic environment.

Steric effects may also play a part in favoring 5c-NO formation. The RR spectrum of the 6c-NO intermediate in AXCP adduct is the first ever reported for a transient 6c-NO hemoprotein. Notably, the 579 cm^{-1} frequency of the ν(Fe−NO) mode is unprecedented, being 20−30 cm^{-1} higher than that of other proteins. As described above, it is possible that the elevated ν(Fe−NO) frequency of AXCP is due to a distorted NO coordination geometry in the distal pocket and that this contributes to the instability of the 6c-NO species. Future studies on 5c- and 6c-NO heme systems should shed light on these issues.

In summary, we have shown that NO binds to ferrous AXCP in a two-step process to form a 6c-NO heme which then converts to a 5c-NO end product. The rates of both the 6c-NO and 5c-NO formation are dependent on the concentration of NO. While the initial NO binding event is consistent with NO coordinating to the distal position, we attribute the NO dependence of the subsequent 6c- to 5c-NO conversion to the attack of a second NO molecule on the proximal side of the heme, to give the proximally bound 5c-NO product observed in the crystal structure. A similar NO binding mechanism, featuring a proximally bound 5c-NO heme, could help to explain the second-order 6c- to 5c-NO conversion previously reported for the heme center in sGC. This alternative model for heme−NO binding offers fresh insights into the mechanism of NO sensing and signal transduction in sGC.

ACKNOWLEDGMENT

We are most grateful to Professor Roger N. F. Thorneley for granting access to kinetic instrumentation and to Dr. Thomas Bruser for assistance with some of the initial experiments on NO binding to AXCP.

REFERENCES

1. Schmidt, H. H. W., and Walter, U. (1994) *Cell 78*, 919−925.
2. Ignarro, L. J. (1996) in *Nitric Oxide: Principles and Actions* (Lancaster, J., Jr., Ed.) pp 111−137, Academic Press, San Diego.
3. Durner, J., Gow, A. J., Stamler, J. S., and Glazebrook, J. (1999) *Proc. Natl. Acad. Sci. U.S.A. 96*, 14206−14207.
4. Watmough, N. J., Butland, G., Cheesman, M. R., Moir, J. W. B., Richardson, D. J., and Spiro, S. (1999) *Biochim. Biophys. Acta 1411*, 456−474.
5. Hutchings, M. I., Shearer, N., Wastell, S., van Spanning, R. J. M., and Spiro, S. (2000) *J. Bacteriol. 182*, 6434−6439.
6. Pohlmann, A., Cramm, R., Schmelz, K., and Friedrich, B. (2000) *Mol. Microbiol. 38*, 626−638.
7. Ding, H., and Demple, B. (2000) *Proc. Natl. Acad. Sci. U.S.A. 97*, 5146−5150.
8. Denninger, J. W., and Marletta, M. A. (1999) *Biochim. Biophys. Acta 1411*, 334−350.
9. Sharma, V. S., and Magde, D. (1999) *Methods 19*, 494−505.

10. Meyer, T. E., and Kamen, M. D. (1982) *Adv. Protein Chem. 35*, 105−212.
11. Moore, G. R., and Pettigrew, G. W. (1990) *Cytochromes c; Evolutionary, Structural and Physicochemical Aspects*, Springer-Verlag, Berlin.
12. Yoshimura, T., Iwasaki, H., Shidara, S., Suzuki, S., Nakahara, A., and Matsubura, T. (1988) *J. Biochem. 103*, 1016−1019.
13. Yoshimura, T., Shidara, S., Ozaki, T., and Kamada, H. (1993) *Arch. Microbiol. 160*, 498−500.
14. Ferguson, S. J. (1991) *Biochim. Biophys. Acta 1058*, 17−20.
15. Moir, J. W. B. (1999) *Biochim. Biophys. Acta 1430*, 65−72.
16. Cross, R., Aish, J., Paston, S. J., Poole, R. K., and Moir, J. W. B. (2000) *J. Bacteriol. 182*, 1442−1447.
17. Cross, R., Lloyd, D., Poole, R. K., and Moir, J. W. B. (2001) *J. Bacteriol. 183*, 3050−3054.
18. Stone, J. R., and Marletta, M. A. (1994) *Biochemistry 33*, 5636−5640.
19. Lawson, D. M., Stevenson, C. E. M., Andrew, C. R., and Eady, R. R. (2000) *EMBO J. 19*, 5661−5671.
20. Makino, R., Matsuda, H., Obayashi, E., Shiro, Y., Iizuka, T., and Hori, H. (1999) *J. Biol. Chem. 274*, 7714−7723.
21. Zhao, Y., Brandish, P. E., Ballou, D. P., and Marletta, M. A. (1999) *Proc. Natl. Acad. Sci. U.S.A. 96*, 14753−14758.
22. George, S. J., Andrew, C. R., Lawson, D. M., Thorneley, R. N. F., and Eady, R. R. (2001) *J. Am. Chem. Soc. 123*, 9683−9684.
23. Ambler, R. P. (1973) *Biochem. J. 1345*, 751−758.
24. Norris, G. E., Anderson, B. F., Baker, E. N., and Rumball, S. V. (1979) *J. Mol. Biol. 135*, 309−312.
25. Cusanovich, M. A., Tedro, S. M., and Kamen, M. D. (1970) *Arch. Biochem. Biophys. 141*, 557−570.
26. Loehr, T. M., and Sanders-Loehr, J. (1993) *Methods Enzymol. 226*, 431−470.
27. Cusanovich, M. A., and Gibson, Q. H. (1973) *J. Biol. Chem. 248*, 822−834.
28. Archer, M., Banci, L., Dikaya, E., and Romão, M. J. (1997) *J. Biol. Inorg. Chem. 2*, 611−622.
29. Spiro, T. G. (1988) in *Biological Applications of Raman Spectroscopy, Vol. 3: Resonance Raman Spectra of Hemes and Metalloproteins* (Spiro, T. G., Ed.) pp 1−37, John Wiley & Sons, New York.
30. Andrew, C. R., Green, E. L., Lawson, D. M., and Eady, R. R. (2001) *Biochemistry 40*, 4115−4122.
31. Howes, B. D., Feis, A., Indiani, C., Marzocchi, M. P., and Smulevich, G. (2000) *J. Biol. Inorg. Chem. 5*, 227−235.
32. Yoshimura, T., Suzuki, S., Nakahara, A., Iwasaki, H., Masuko, M., and Matsubara, T. (1985) *Biochim. Biophys. Acta 831*, 267−274.
33. Strekas, T. C., and Spiro, T. G. (1974) *Biochim. Biophys. Acta 351*, 237−245.
34. Kitagawa, T., Ozaki, Y., Kyooku, Y., and Horio, T. (1977) *Biochim. Biophys. Acta 495*, 1−11.
35. Hobbs, J. D., Larsen, R. W., Meyer, T. E., Hazzard, J. H., Cusanovich, M. A., and Ondrias, M. R. (1990) *Biochemistry 29*, 4166−4174.
36. Othman, S., Richaud, P., Verméglio, A., and Desbois, A. (1996) *Biochemistry 35*, 9224−9234.
37. Tomita, T., Hirota, S., Ogura, T., Olson, J. S., and Kitagawa, T. (1999) *J. Phys. Chem. B 103*, 7044−7054.
38. Ding, X. D., Weichsel, A., Andersen, J. F., Shokhireva, T. K., Balfour, C., Pierik, A. J., Averill, B. A., Montfort, W. R., and Walker, F. A. (1999) *J. Am. Chem. Soc. 121*, 128−138.
39. Vogel, K. M., Kozlowski, P. M., Zgierski, M. Z., and Spiro, T. G. (1999) *J. Am. Chem. Soc. 121*, 9915−9921.
40. Wondimagegn, T., and Ghosh, A. (2001) *J. Am. Chem. Soc. 123*, 5680−5683.
41. Stone, J. R., and Marletta, M. A. (1996) *Biochemistry 35*, 1093−1099.
42. Vogel, K. M., Hu, S., Spiro, T. G., Dierks, E. A., Yu, A. E., and Burstyn, J. N. (1999) *J. Biol. Inorg. Chem. 4*, 804−813.
43. Reynolds, M. F., Parks, R. B., Burstyn, J. N., Shelver, D., Thorsteinsson, M. V., Kerby, R. L., Roberts, G. P., Vogel, K. M., and Spiro, T. G. (2000) *Biochemistry 39*, 388−396.
44. Traylor, T. G., and Sharma, V. S. (1992) *Biochemistry 31*, 2847−2849.
45. Scheidt, W. R., and Ellison, M. K. (1999) *Acc. Chem. Res. 32*, 350−359.
46. Kharitonov, V. G., Sharma, V. S., Magde, D., and Koesling, D. (1997) *Biochemistry 36*, 6814−6818.
47. Yoshimura, T., Fujii, S., Kamada, H., Yamaguchi, K., Suzuki, S., Shidara, S., and Takakuwa, S. (1996) *Biochim. Biophys. Acta 1292*, 39−46.
48. Lukat-Rodgers, G. S., and Rodgers, K. R. (1997) *Biochemistry 36*, 4178−4187.
49. Schelvis, J. P. M., Seibold, S. A., Cerda, J. F., Garavito, R. M., and Babcock, G. T. (2000) *J. Phys. Chem. B 104*, 10844−10850.
50. Deinum, G., Stone, J. R., Babcock, G. T., and Marletta, M. A. (1996) *Biochemistry 35*, 1540−1547.
51. Tomita, T., Ogura, T., Tsuyama, S., Imai, Y., and Kitagawa, T. (1997) *Biochemistry 36*, 10155−10160.
52. O'Keefe, D. H., Ebel, R. E., and Peterson, J. A. (1978) *J. Biol. Chem. 253*, 3509−3516.
53. Yonetani, T., Yamamoto, H., Erman, J. E., Leigh, J. S., and Reed, G. H. (1972) *J. Biol. Chem. 247*, 2447−2455.
54. Butt, W. D., and Keilin, D. (1962) *Proc. R. Soc. London, Ser. B 156*, 429−458.
55. Iwasaki, H., Yoshimura, T., Suzuki, S., and Shidara, S. (1991) *Biochim. Biophys. Acta 1058*, 79−82.
56. Moore, E. G., and Gibson, Q. H. (1976) *J. Biol. Chem. 251*, 2788−2794.
57. Hoshino, M., Ozawa, K., Seki, H., and Ford, P. (1993) *J. Am. Chem. Soc. 115*, 9568−9575.
58. Duprat, A. F., Traylor, T. G., Wu, G.-Z., Coletta, M., Sharma, V. S., Walda, K. N., and Magde, D. (1995) *Biochemistry 34*, 2634−2644.
59. Yoshimura, T., and Suzuki, S. (1988) *Inorg. Chim. Acta 152*, 241−249.
60. Tsubaki, M., and Yu, N. T. (1982) *Biochemistry 21*, 1140−1144.
61. Hu, S., and Kincaid, J. R. (1991) *J. Am. Chem. Soc. 113*, 9760−9766.
62. Hu, S., and Kincaid, J. R. (1993) *J. Biol. Chem. 268*, 6189−6193.
63. Wang, J., Rousseau, D. L., Abu-Soud, H. M., and Stuehr, D. J. (1994) *Proc. Natl. Acad. Sci. U.S.A. 91*, 10512−10516.
64. Fan, B., Gupta, G., Danziger, R. S., Friedman, J., and Rousseau, D. L. (1998) *Biochemistry 37*, 1178−1184.

BI011419K